
Enhanced performance of piezoelectric energy harvester by two asymmetrical splitter plates

Junlei Wang ^a, Bing Xia ^a, Daniil Yurchenko ^b, Grzegorz Litak ^c, Yong Li ^d, Haigang Tian ^{a,*}

^a School of Mechanical and Power Engineering, Zhengzhou University, Zhengzhou 450000, China;

^b Institute of Sound and Vibration Research, University of Southampton, SO17 1BJ, UK;

^c Department of Automation, Lublin University of Technology, Nadbystrzycka 36, PL-20-618 Lublin, Poland;

^d School of Electrical Engineering, Southwest Jiaotong University, Chengdu 610031, China

*Corresponding author: Haigang Tian, E-mail address: tianhaigang@zzu.edu.cn.

Abstract: This paper proposes a novel vortex-induced vibration piezoelectric energy harvester attached to two asymmetrical splitter plates (VIVPEH-S), which aims at converting the vibration mode from vortex-induced vibration (VIV) to galloping and improving the energy harvesting efficiency. The conceptual designing of VIVPEH-S with two asymmetrical splitter plates under various installation angles is first conducted, the experimental prototypes are then fabricated and the wind tunnel experimental system is constructed, and the simulation model of the harvester system is finally established. The effects of the installation angles of two asymmetrical splitter plates on the vibration characteristics and harvesting performance of VIVPEH-S are experimentally investigated, and the vortex shedding characteristic and mode conversion mechanism are revealed by CFD simulation. The results demonstrate that the installation of the asymmetrical splitter plates changes the vortex shedding characteristics, transforms the vibration mode from VIV to galloping, which can significantly broaden the working bandwidth, and improves the energy harvesting performance. A maximum enhancement ratio of the output power of VIVPEH-S with $\alpha = 60^\circ$ and $\beta = 90^\circ$ is up to 471.2% over the conventional VIVPEH. This work provides an important foundation for designing a more efficient piezoelectric energy harvester by using asymmetrical splitter plates.

Keywords: energy harvesting; vortex-induced vibration; galloping; asymmetrical splitter plates; enhanced performance

1 **1. Introduction**

2 The vibration-into-energy harvesting technology from the natural environment
3 has been investigated in recent years [1-7], aiming to replace the conventional battery
4 for driving the low-power wireless sensor system usually placed in a remote location
5 and reducing carbon footprints [8-11]. Flow-induced vibration (FIV) energy
6 harvesting is considered an alternative to renewable wind energy technology that
7 captures energy from the low-speed [air](#)flow environment [12-17]. It converts the fluid
8 kinetic energy into electrical energy to drive electrical equipment, for example,
9 wireless sensors and micro-electromechanical systems [13, 18, 19]. [The FIV-based](#)
10 [energy harvester can convert wind energy into electricity using piezoelectric-](#) [14, 20-
11 [22\], electromagnetic \[23, 24\], electrostatic \[25-27\], and triboelectric \[28-30\]. Because](#)
12 [of simple structure, low cost, and high power density, piezoelectric energy harvesters](#)
13 [have become a research hotspot in recent decades.](#)

14 The efficiency of the energy harvester based on FIV is higher than that of the
15 [traditional energy harvesters by using heat, light, and electromagnetic,](#) ~~and it~~ has
16 [been extensively studied by some scholars in recent decades \[31-33\].](#) The common
17 FIV phenomenon includes vortex-induced vibration (VIV) [13, 20, 30], galloping [29,
18 34], wake galloping [35, 36], and flutter [37-39]. But VIV-based piezoelectric energy
19 harvester (VIVPEH) can only collect substantial energy in the lock-in region [24, 40,
20 41]. [Therefore, to improve the energy harvesting efficiency of VIVPEH, some](#)
21 [methods, widening the lock-in region \[42, 43\], introducing the nonlinear forces \[44,](#)
22 [45\], and adding the degrees of freedom \[46-48\], have been adopted by many](#)
23 [researchers. Zhang et al. \[49\] explored the effect of placing a fixed cylinder](#)
24 [downstream on the energy ~~capture~~-\[harvesting\]\(#\) characteristics, and the experimental](#)
25 [results show that the presence of the downstream fixed cylinder can not only](#)
26 [improve the wind speed range of energy harvesting, but also increase the maximum](#)
27 [output power by 1500%. Franzini and Bunzel \[46\] added an extra degree of freedom](#)
28 [based on the original device, and increased energy capture efficiency by 50-%.](#)

29 However, it is worth noting that some authors have paid more attention to the
30 [performance improvement of energy harvesters, but have not studied the internal](#)
31 [mechanisms, such as vortex shedding of fluid flow.](#) Compared with VIV, galloping
32 does not have a lock-in region [50-52], and the range of wind speeds available for

1 energy harvesting is also wider [53-55]. Therefore, the vast majority of recent
2 research has been focused on changing the vibration mode of the bluff body, such as
3 adding accessories to the structure of the bluff body to promote the conversion of VIV
4 into galloping. Compared with VIV, galloping can increase the strength of the
5 vibration and widen the wind speed range to improve the efficiency of energy
6 harvesting [43, 44, 56]. Song et al. [57] added a single splitter plate with different
7 lengths ~~on~~ to VIVPEH and demonstrated that adding the splitter plate can eliminate
8 the performance limitation of VIV in the lock-in region. The vibration behaves as
9 galloping at the splitter plate of exceeding a certain length. Therefore, compared with
10 the conventional VIVPEH, it can capture energy over a wider range of wind speeds
11 and improve the efficiency of energy harvesting. However, previous studies neither
12 discussed the optimal installation position of the splitter plate to maximize the
13 performance of the energy harvester nor fully investigated the conversion mechanism
14 from VIV to galloping from the perspective of wake vorticity changes and structural
15 morphology. Hu et al. [34] studied the method of adding small cylindrical appendages
16 to the bluff body for improving the efficiency of the energy harvester. The
17 experimental result ~~shows~~ shown that indicating the rods installed at $\theta = 60^\circ$, the
18 vibration mode ~~can be~~ changed from VIV to galloping and greatly ~~increas~~ ed the
19 wind speed range and the output power. Wang et al. [58] ~~made the vibration mode~~
20 ~~transition from VIV to galloping by adding Y-shaped accessories to the blunt body,~~
21 ~~thereby greatly improving energy harvesting efficiency.~~ Unfortunately, the internal
22 mechanism of the transformation from VIV to galloping vibration has not been well
23 discussed. Wang et al. [59] then studied the effect of adding a symmetric splitter plate
24 to a cylindrical bluff body on the efficiency of the energy harvester. The research
25 showed that the energy harvesting efficiency reached its peak when the angle between
26 the symmetrical splitter plates and the blunt cylinder was 60° , and the formation
27 length of the vortex increased with the increase of the installation angle. However, the
28 influence of asymmetrical splitter plates on output characteristics was not investigated
29 in this study. The flow field and vibration characteristics of two asymmetrical splitter
30 plates were largely different from that of symmetrical ones.

31 As can be known from the above overviews that adding accessories or splitter
32 plates to the cylindrical bluff body could convert the vibration mode from VIV to
33 galloping, which enhanced the energy harvesting efficiency of piezoelectric energy

1 harvesters [60, 61]. Most of the existing literature mainly focused on adding
2 symmetric splitter plates ~~on~~ to the bluff body and finally exploring the effect on
3 energy harvesting efficiency. The installation of the symmetrical splitter plates on the
4 cylindrical bluff body can significantly improve its energy harvesting effect compared
5 ~~to~~ with the conventional VIVPEH. However, VIVPEH with two asymmetrical splitter
6 plates at different installation angles has not been explored up to now. Compared with
7 the symmetrical splitter plates, two asymmetrical splitter plates installed on the
8 cylindrical bluff body demonstrated a marked difference in the flow field and
9 vibration characteristics. The harvesting efficiency of the piezoelectric energy
10 harvester with two asymmetrical splitter plates and the conversion mechanism of VIV
11 to galloping have not been analyzed in detail. There is a necessity to investigate the
12 conversion mechanism, vibration characteristics, and harvesting performance of the
13 piezoelectric energy harvester with two asymmetrical splitter plates, for promoting the
14 actual applications in the natural environment.

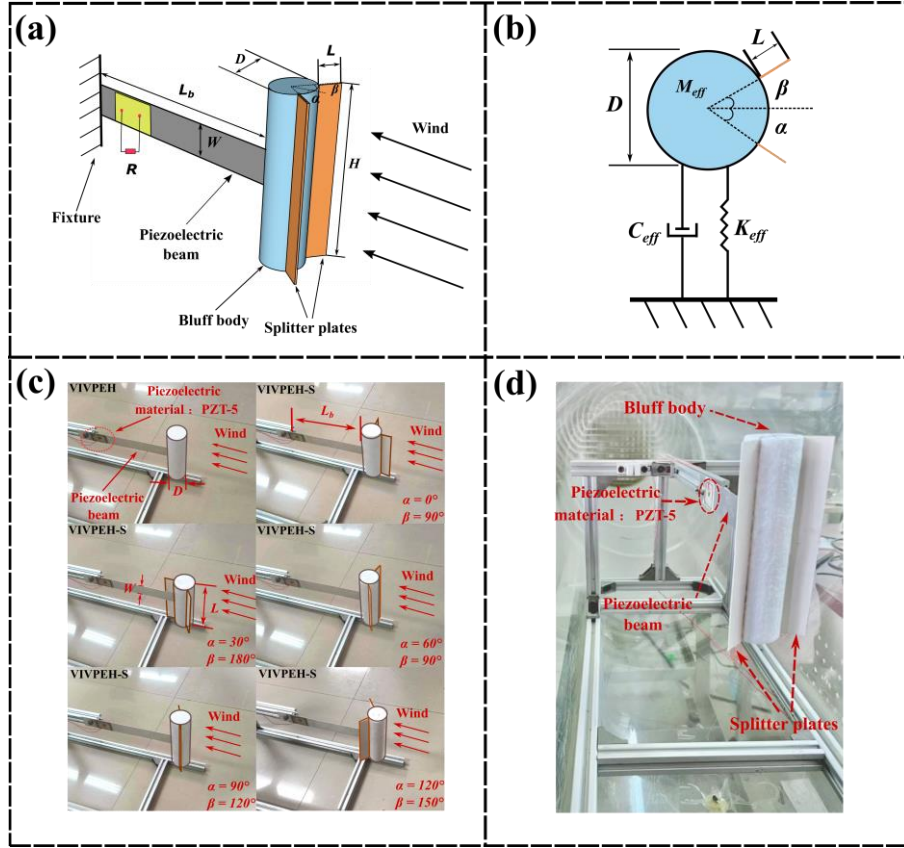
15 Therefore, the main content of this paper is to determine the best installation
16 angle of adding two asymmetrical splitter plates to the cylindrical bluff body, increase
17 energy capturing efficiency and broaden the wind speed range. The contributions of
18 this paper are as follows: (1) A novel vortex-induced vibration piezoelectric energy
19 harvester with two asymmetrical splitter plates (VIVPEH-S) is first proposed; (2) The
20 optimal installation angles of two asymmetrical splitter plates are obtained, which
21 improved the energy harvesting performance; (3) The underlying mechanism of the
22 vortex shedding mode and the conversion mechanism are reveal; (4) A maximum
23 enhancement ratio of the output power of VIVPEH-S with $\alpha = 60^\circ$ and $\beta = 90^\circ$ is
24 increased by 471.2% over the conventional VIVPEH.

25 The structure of this paper is as follows: conceptual designing and prototype
26 fabrication of VIVPEH-S are conducted, and the vibration characteristics and
27 harvesting performance of [the harvester attached to](#) two asymmetrical splitter plates at
28 various installation angles are experimentally investigated in Section 2. The flow field
29 characteristic and conversion mechanisms are revealed by using CFD simulation
30 analyses in Section 3. Some important conclusions of this paper are drawn in Section
31 4.

2. Design, analyses, and discussions of VIVPEH-S

2.1. Conceptual design and prototype fabrication

The designed vortex-induced vibration piezoelectric energy harvester with two asymmetrical splitter plates (VIVPEH-S) device is mainly composed of a cylindrical bluff body equipped with two asymmetrical splitter plates, a piezoelectric beam, and a piezoelectric sheet. The aimss are to convert the vibration mode from VIV into galloping and improve the harvesting performance. In this system, the piezoelectric sheet is first bonded near the fixed end of the piezoelectric beam, and the piezoelectric beam is connected to the bluff body and then placed in the wind tunnel. When the fluid passes by the cylindrical bluff body with two asymmetrical splitter plates, the flow-induced vibration phenomenon occurs, which drives the piezoelectric beam to vibrate back and forth, and finally converts the wind energy into electrical energy through the piezoelectric sheet. Figure 1 illustrates the design, model, and prototype of VIVPEH-S. Figure 1 (a) shows a three-dimensional schematic diagram of VIVPEH-S. The length, width, and thickness of the aluminum cantilever are $L \times W \times h_b = 164 \text{ mm} \times 24 \text{ mm} \times 0.5 \text{ mm}$. The cylindrical bluff body is made of rigid plastic foam, with height H , and diameter D of 118 mm, and 32 mm, respectively. The piezoelectric sheet PZT-5 (Jiayeshi Co, China) with length, width, and thickness are 30 mm, 20 mm, and 0.5 mm, respectively. Table 1 lists the main material parameters of PZT-5. Figure 1 (b) illustrates the equivalent model of VIVPEH-S. Therein, the angles between the two splitter plates installed in the center of the cylindrical bluff body and the incoming flow direction are, respectively, defined as α and β . The actual model of the conventional VIVPEH and VIVPEH-S is shown in Figure 1 (c). The wind tunnel experimental setup is shown in Figure 1 (d). The model of VIVPEH-S is installed in a wind tunnel and the diameter of the wind tunnel is 0.4 m. In this experiment, different wind speeds can be generated by controlling the speed of the induced draft fan, and the wind speed ranges from 0.73 m/s to 2.51 m/s. The natural frequencies of VIVPEH and VIVPEH-S are about 7.89 Hz, which can be obtained through the free vibration attenuation experiment. The voltage during the experiment is recorded by the data acquisition device in the form of alternating current and used to obtain the output power.



1
2 **Figure 1.** VIVPEH-S configuration: (a) Schematic diagram of VIVPEH-S; (b) Equivalent model
3 of VIVPEH-S; (c) The VIVPEH and VIVPEH-S prototypes with different angles α and β ; (d)
4 Wind tunnel experimental device.

5 **Table 1.** Material parameters of PZT-5

Physical parameter	Values
Density (ρ) [kg/m ³]	7500
Stiffness (c_{11}^E) [GPa]	56
Capacitance (C_p) [nF]	30.16
Electromechanical coupling factors (K_p)	0.68
Dielectric constants (ϵ_r) [1 kHz]	3200

6 The experimental processes of this paper are as follows: First, the flow speed
7 was adjusted by changing the rotation frequency of the induced draft fan, and the
8 experiment begins when the wind speed was calibrated. Second, an error analysis is
9 performed on the measured voltage to ensure that accurate experimental results are
10 obtained, and then measure the root means square (RMS) of the output voltage in the
11 experimental wind speed range. The last step is to repeatedly measure the RMS
12 voltages of the VIVPEH-S at different wind speeds. It should be noted that the mass

of the cylindrical bluff body with asymmetrical splitter plates should be carefully calibrated before the experiment to calculate the equivalent mass of the whole device.

Figure 2 illustrates six groups of VIVPEH-S with varying α and β . To avoid the situation of the repeated experimental groups concerning the cylinder axis symmetry, the selected variable angle α ranges from 0° to 150° , and the corresponding β ranges from 30° to 180° . Before the experiment, a series of angles of the manifold are tested, and the difference between α and β at various test groups was finally selected based on a multiple of 30° [59]. In addition, the choice of the numerical value of the installation angle is based on comprehensive experimental conditions and ensures that the experimental phenomenon can be effectively explored. The effects of the installation angles of two asymmetrical splitter plates on the output characteristics of VIVPEH-S are fully investigated in the following analyses.

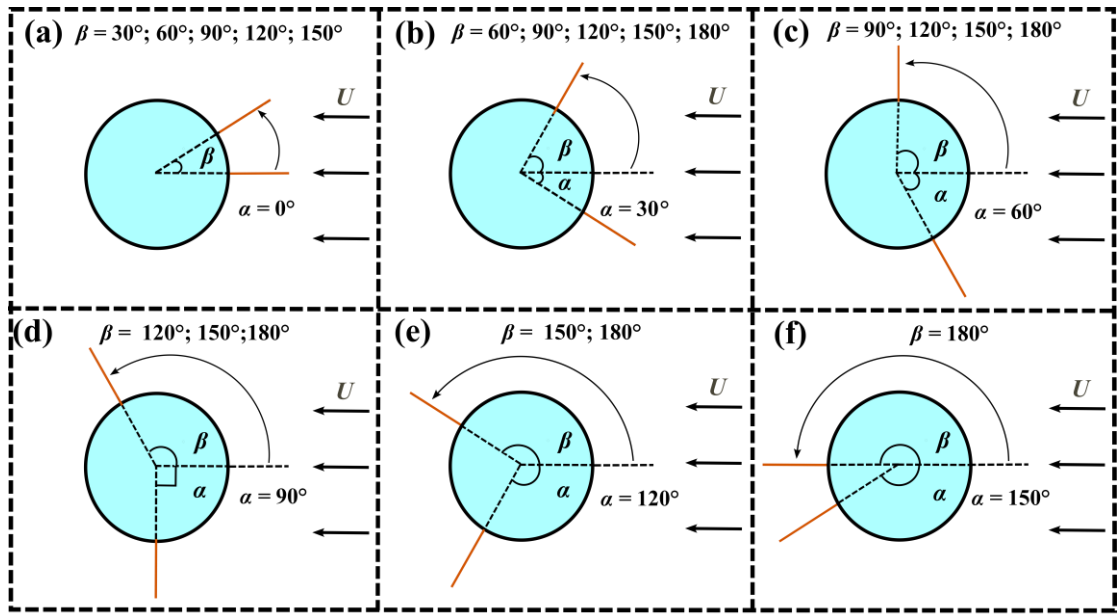
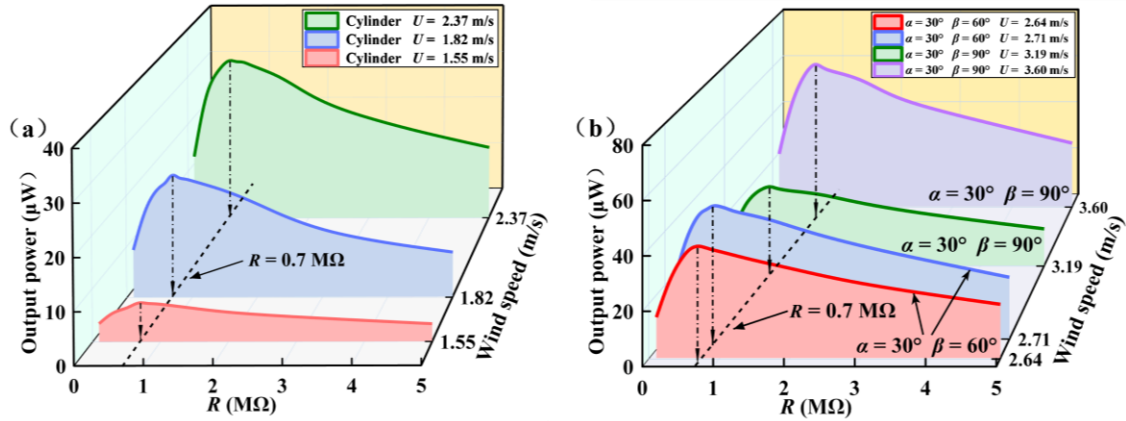


Figure 2. Six groups of VIVPEH-S with varying α and β .

2.2. Results and discussions

To evaluate the vibration characteristics and harvesting performance of VIVPEH-S and pursue better output characteristics, the external load resistance should be first matched. Therein, output power $P = V_{rms}^2 / R$; V_{rms} represents the RMS output voltage; R represents the external load resistance. Figure 3 shows the output

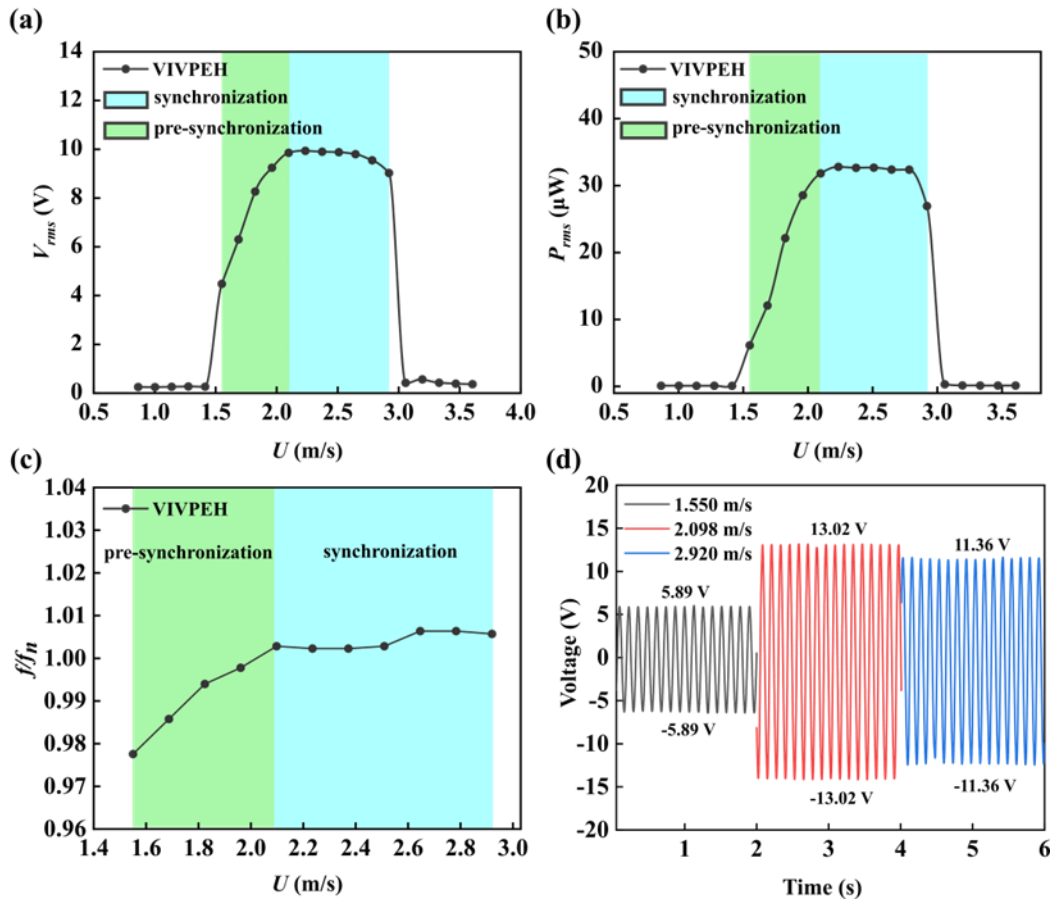
1 power of VIVPEH-S and the conventional VIVPEH. The obtained output power first
 2 increases until the peak values are attained and then decreases with the increase of the
 3 load resistance at the considered wind speed. The optimal load resistance of 0.7 M Ω is
 4 obtained, at which the output power of both VIVPEH and VIVPEH-S reaches their
 5 maximum values. Therefore, the optimal load resistance R_{opt} of 0.7 M Ω for VIVPEH
 6 and VIVPEH-S is selected in the following experimental investigation.



7
 8 **Figure 3.** The output power with the load resistance at various wind speeds: (a) conventional
 9 VIVPEH; (b) VIVPEH-S with $\alpha = 30^\circ$.

10 To highlight the effect of the added two asymmetrical splitter plates on the
 11 harvesting performance of VIVPEH-S and conduct the comparative analyses, the
 12 output characteristics of the conventional VIVPEH should be first investigated. Figure
 13 4 illustrates the output characteristics of the conventional VIVPEH. Figure 4 (a)
 14 shows that with the increase of wind speed, the output voltage first approaches 0 V,
 15 and increases rapidly when the wind speed is greater than 1.69 m/s. It reaches a stable
 16 state again in the interval of wind speed from 2.24 m/s to 2.92 m/s, and then decreases
 17 rapidly and finally reaches a stable state. The lock-in phenomenon can be observed
 18 from 2.24 m/s to 2.92 m/s, and when the wind speed is 2.372 m/s, the maximum RMS
 19 output voltage is 9.93 V. Figure 4 (b) shows the change curve of the output power of
 20 VIVPEH with the wind speed. The changing trend is almost the same as the output
 21 voltage. Therefore, the output power of the conventional VIVPEH outside the lock-in
 22 regions is limited, which can only provide satisfactory performance in a limited range
 23 of wind speeds. To further explore the internal principle of the lock-in region, Figure
 24 4 (c) shows the dimensionless frequency change curve of VIVPEH with the wind
 25 speed. When the wind speed is between 1.550 m/s and 2.098 m/s, the dimensionless

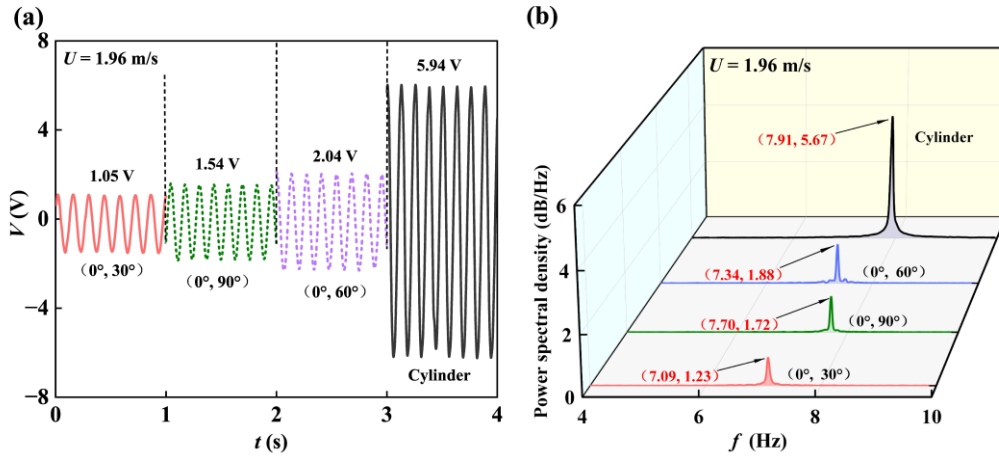
1 frequency increases with the increase of the wind speed, this phenomenon is pre-
 2 synchronization and is represented by the green area. When the wind speed ranges
 3 from 2.098 m/s to 2.509 m/s, the curve remains almost horizontal, the value of the
 4 dimensionless frequency is equal to 1, and this phenomenon is called synchronization
 5 and is represented by the blue area. Figure 4 (d) shows the output voltage time-history
 6 curve at 1.69 m/s, 2.24 m/s, and 2.92 m/s, respectively. Therein, three wind speeds are
 7 selected, which correspond to the vortex-induced initial excitation branch, upper
 8 branch, and lower branch. Compared with the galloping, there exists the lock-in
 9 interval limit during the vibration process, therefore, larger voltage values can be
 10 obtained at the lock-in region, such as 2.098 m/s.



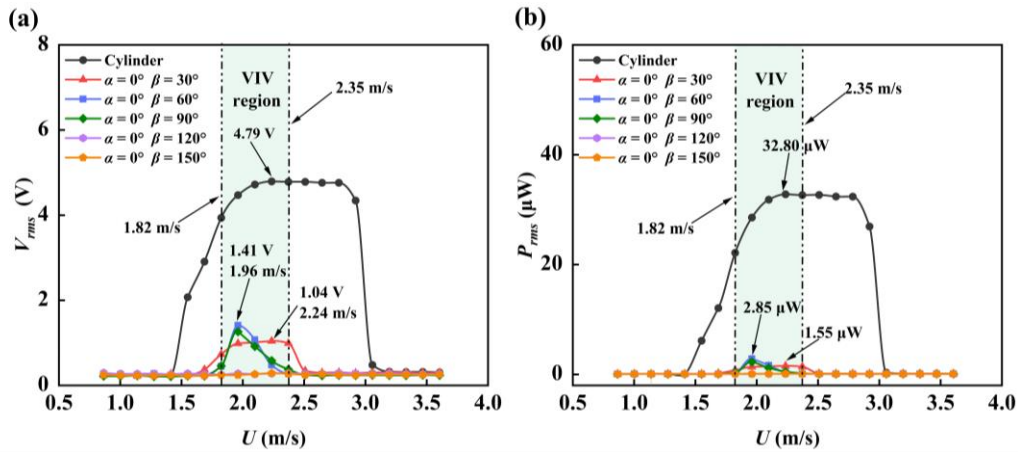
11
 12 **Figure 4.** Output characteristics of the conventional VIVPEH: (a) Variation of the output voltage
 13 with the wind speed; (b) Variation of the output power with the wind speed; (c) Dimensionless
 14 frequency with different wind speeds; (d) Time histories of the output voltage at 1.550 m/s, 2.098
 15 m/s, and 2.920 m/s.

16

1 To explore the influence of the installation angle of two asymmetrical splitter
 2 plates on the output voltage, the VIVPEH-S with $\alpha = 0^\circ$ ($\beta = 30^\circ, \beta = 60^\circ, \beta = 90^\circ, \beta$
 3 $= 120^\circ$, and $\beta = 150^\circ$) are selected. Figures 5 and 6 shows the vibration characteristic
 4 and harvesting performance of the VIVPEH and VIVPEH-S with $\alpha = 0^\circ$ under the
 5 optimal load resistance. Therein, the adopted output voltage performs the time history
 6 and Fast Fourier Transform (FFT) analyses, to demonstrate the vibration
 7 characteristics.



8
 9 **Figure 5.** Vibration characteristic of VIVPEH-S with $\alpha = 0^\circ$ and the conventional VIVPEH: (a)
 10 Time history; (b) FFT analyses.



11
 12 **Figure 6.** Harvesting performance of VIVPEH-S with $\alpha = 0^\circ$ and the conventional VIVPEH: (a)
 13 Output voltage; (b) Output power.

14 As can be observed from Figure 5 (a) that VIVPEH and VIVPEH-S with $\alpha = 0^\circ$
 15 demonstrate the constant amplitude and periodic vibration at 1.96 m/s. The vibration

1 amplitude of VIVPEH-S with $\alpha = 0^\circ$ is smaller than that of the conventional VIVPEH.
 2 Figure 5 (b) shows that the vibration frequency of the conventional VIVPEH is
 3 slightly higher than that of VIVPEH-S with $\alpha = 0^\circ$. It means that the installation of
 4 two asymmetrical splitter plates largely affects the vibration response, while, the
 5 installation angles play less impact on the frequency. Figure 6 (a) shows the output
 6 voltage of VIVPEH-S with $\alpha = 0^\circ$ and $\beta = 30^\circ$ reaches a peak value of 1.04 V when
 7 the wind speed is 2.23 m/s, its maximum output power is 1.55 μW , and its variation
 8 curve demonstrates the significant VIV characteristics. When $\alpha = 0^\circ$ and $\beta = 90^\circ$, the
 9 output voltage of VIVPEH-S reaches the maximum value of 1.26 V at 1.96 m/s, and
 10 its maximum output power is 2.27 μW . When $\alpha = 0^\circ$, the maximum output voltages
 11 and output power of VIVPEH-S with β of 60° are 1.41 V and 2.85 μW , respectively.
 12 While the output voltage and output power are almost negligible at β of 120° and
 13 150° . It can be found that the output voltage of VIVPEH-S with $\alpha = 0^\circ$ at different
 14 wind speeds is smaller than the conventional VIVPEH, and it can be judged from the
 15 changing trends of output voltage and power that its vibration mode still demonstrates
 16 VIV. While certain installation angles of two asymmetrical splitter plates demonstrate
 17 a suppressing effect on VIV. It is wise not to adopt α of 0° in designing the harvester
 18 system.

19 The installation angle α of the splitter plates exerts an essential role in the output
 20 characteristics of VIVPEH-S. VIVPEH-S with $\alpha = 30^\circ$ ($\beta = 60^\circ, \beta = 90^\circ, \beta = 120^\circ, \beta$
 21 $= 150^\circ$, and $\beta = 180^\circ$) is also adopted. Figures 7 and 8 shows the vibration
 22 characteristic and harvesting performance of the conventional VIVPEH and VIVPEH-
 23 S with $\alpha = 30^\circ$ under the optimal load resistance.

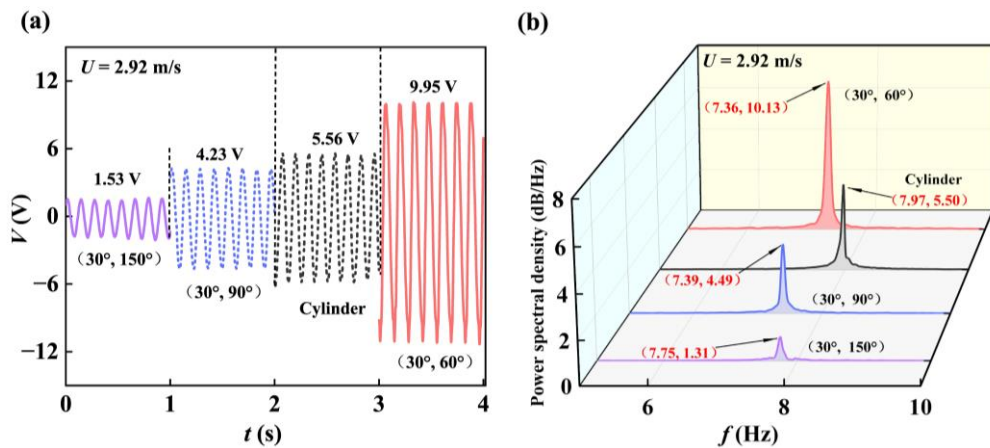


Figure 7. Vibration characteristic of VIVPEH-S with $\alpha = 30^\circ$ and the conventional VIVPEH: (a)

Time history.

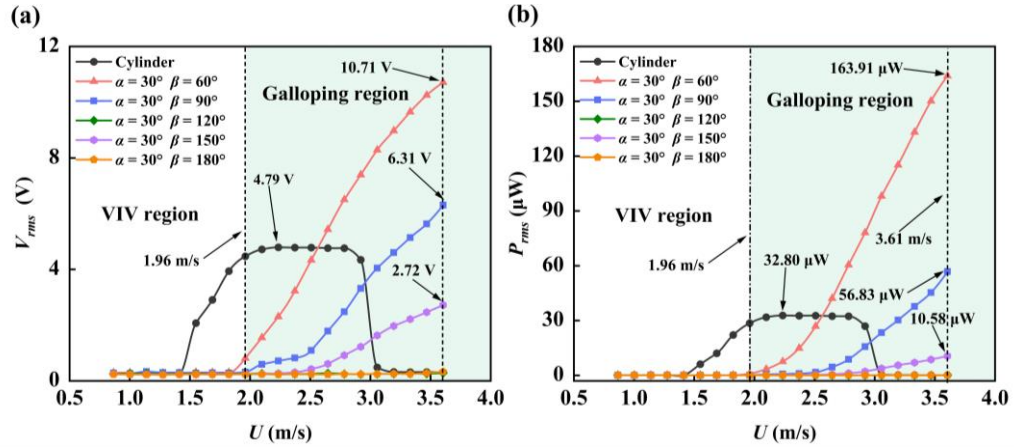
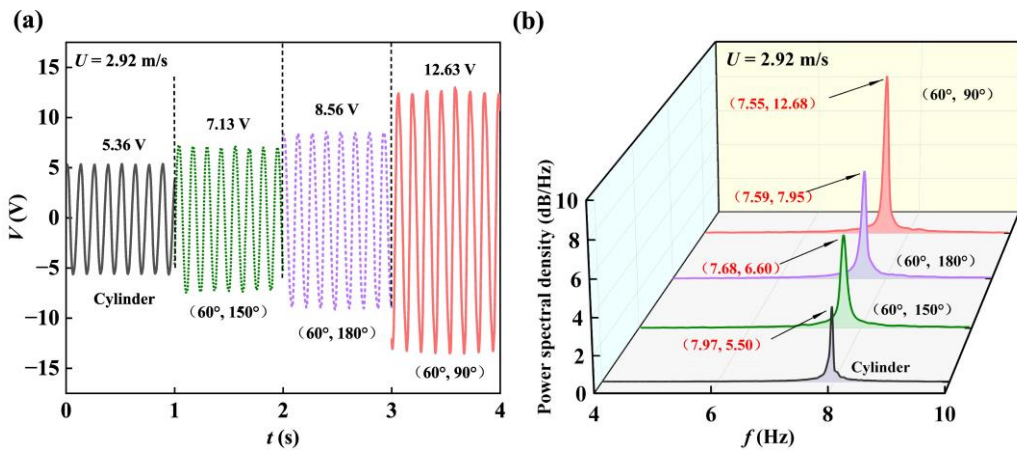


Figure 8. Harvesting performance of VIVPEH-S with $\alpha = 30^\circ$ and the conventional VIVPEH: (a) Output voltage; (b) Output power.

1 The amplitude of the output voltage of the conventional VIVPEH is 5.56 V when
2 the wind speed is 2.92 m/s. While, 9.95 V for VIVPEH-S with $\alpha = 30^\circ$ and $\beta = 60^\circ$. It
3 means that the added two asymmetrical splitter plates enhance the vibration response.
4 The vibration frequency of VIVPEH-S with $\alpha = 30^\circ$ increases with the increase of the
5 installation angle β , which is lower than that of the conventional VIVPEH. For
6 VIVPEH-S with $\alpha = 30^\circ$ and $\beta = 60^\circ$, the maximum output voltage is up to 10.71 V,
7 which is 123.60% higher than 4.79 V of the conventional VIVPEH. And its peak
8 output power is 163.91 μW , which is 399.7% higher than the 32.80 μW of the
9 conventional VIVPEH. Therefore, the promotion effect of its energy harvesting
10 performance is obvious from this installation angle. For VIVPEH-S with $\alpha = 30^\circ$ and
11 $\beta = 90^\circ$, the maximum output power is 56.83 μW , and the enhanced ratio is up to
12 73.2%. When the wind speed is greater than 1.96 m/s, the vibration modes of the test
13 group all demonstrate galloping, it can be concluded from the characteristic of
14 galloping that the lower the starting wind speed within the tested wind speed range is,
15 the better the vibration characteristic and energy harvesting performance can be
16 obtained. **The conventional VIVEPH can obtain a better energy harvesting**
17 **performance in its locked-in region, and its effective energy harvesting wind speed**
18 **range is $U = 1.55$ m/s - 2.92 m/s. While, the effective energy harvesting wind speed**
19 **range of VIVEPH-S is $U = 1.96$ m/s - 3.60 m/s within the experimental wind speed.**
20 **Therefore, its effective harvesting energy working bandwidth increased by 19.7%.**
21 Compared with the conventional VIVPEH, the other VIVPEH-S in the same group

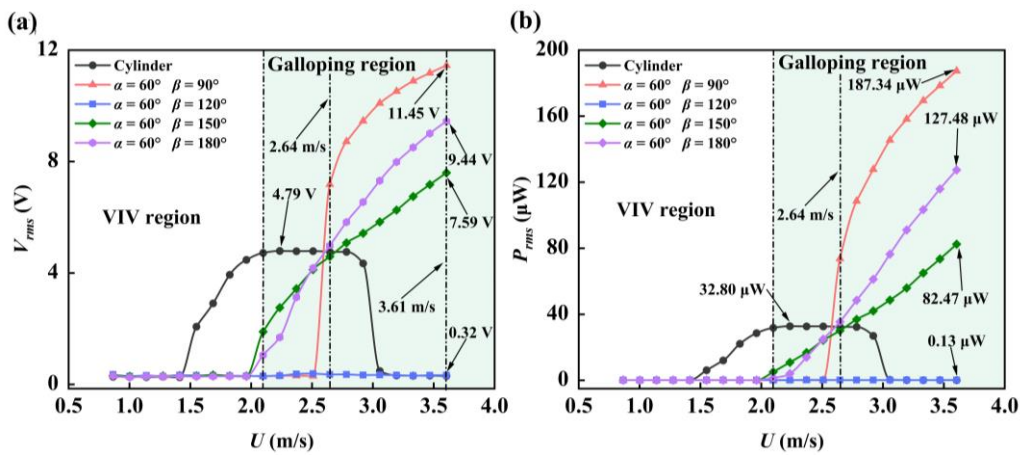
1 shows the inhibition effect in energy harvesting performance, the output voltage of
 2 VIVPEH-S with $\alpha = 30^\circ$ and $\beta = 150^\circ$ reaches a peak value of 2.72 V, and its
 3 maximum output power is $10.58 \mu\text{W}$. While the output voltage and output power are
 4 almost negligible at β of 120° and 180° . Therefore, adopting $\alpha = 30^\circ$ and $\beta = 60^\circ$, the
 5 VIVPEH-S can harvest better output characteristics.

6 When the installation angle α is 60° , VIVPEH-S with $\alpha = 60^\circ$ ($\beta = 90^\circ, \beta = 120^\circ,$
 7 $\beta = 150^\circ,$ and $\beta = 180^\circ$) is selected. Figures 9 and 10 shows the output characteristics
 8 of the conventional VIVPEH and VIVPEH-S with $\alpha = 60^\circ$ under the optimal load
 9 resistance as a function of the wind speed.



10

11 **Figure 9.** Vibration characteristic of VIVPEH-S with $\alpha = 60^\circ$ and the conventional VIVPEH: (a)
 12 Time history; (b) FFT analyses.



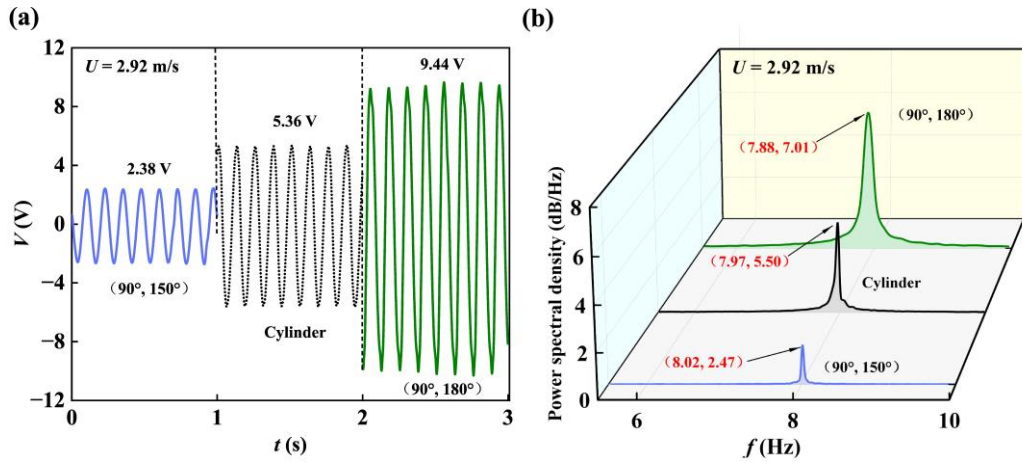
13

14 **Figure 10.** Harvesting performance of VIVPEH-S with $\alpha = 60^\circ$ and the conventional VIVPEH: (a)
 15 Output voltage; (b) Output power.

1 As can be known from Figure 9 (a) that the vibration amplitudes of VIVPEH-S
2 at considered installation angles are all larger than that of the conventional VIVPEH.
3 It means that adding the asymmetrical splitter plates to the cylindrical bluff body can
4 enhance the vibration amplitude to some extent. Figure 9 (b) demonstrates that the
5 added asymmetrical splitter plates exert less effect on the mass, and thus there exists a
6 small difference in the vibration frequency for VIVPEH-S. Figure 10 (a) demonstrates
7 the corresponding output voltages of VIVPEH-S with $\alpha = 60^\circ \beta = 90^\circ$, $\alpha = 60^\circ \beta =$
8 150° , and $\alpha = 60^\circ \beta = 180^\circ$ under the optimal load resistance are 11.45 V, 7.59 V, and
9 9.44 V, respectively. The peak output voltages are significantly larger than that of the
10 conventional VIVPEH. It can be concluded from Figure 10 (b) that the peak output
11 powers of the above three groups are 187.34 μW , 82.47 μW , and 127.48 μW ,
12 respectively. The energy harvesting performance of three VIVPEH-S is increased by
13 471.2%, 151.4%, and 288.7% compared with the conventional VIVPEH. Moreover,
14 when the wind speed is only 2.64 m/s, the energy harvester with $\alpha = 60^\circ$ and $\beta = 90^\circ$
15 started to vibrate, and its voltage shows a jumping increase compared with others.
16 Compared with other VIVPEH-S, the output voltage and output power of VIVPEH-S
17 with $\alpha = 60^\circ$ and $\beta = 120^\circ$ are only 0.32 V and 0.13 μW , respectively, and the energy
18 harvesting performance is suppressed.

19 For the installation angle α of 90° , VIVPEH-S with $\alpha = 90^\circ$ ($\beta = 120^\circ$, $\beta = 150^\circ$,
20 and $\beta = 180^\circ$) is adopted. Figures 11 and 12 shows the output characteristics of the
21 conventional VIVPEH and VIVPEH-S with $\alpha = 90^\circ$ at different wind speeds. As can
22 be known from Figure 11 (a) that adopting various installation angles demonstrate a
23 marked difference in output voltage. The output voltage of VIVPEH-S with $\alpha = 90^\circ$
24 and $\beta = 180^\circ$ is up to 9.44 V at 2.92 m/s. Figure 11 (b) shows that there exists a small
25 difference in the vibration frequency for various harvesters. When β is equal to 150°
26 and 180° , the peak output voltages are 2.26 V and 0.29 V, respectively. And the
27 energy harvesting performance is suppressed. The energy harvesting performance of
28 the corresponding energy harvester is suppressed due to the existence of two
29 asymmetrical splitter plates. Noting that when α is equal to 90° , the output voltages
30 increase with the increase of β angle, and its energy harvesting performance is also
31 improved. The peak output voltage of VIVPEH-S with $\alpha = 90^\circ$ and $\beta = 180^\circ$ under the
32 optimal load resistance is 10.25 V, which is significantly larger than that of the
33 conventional VIVPEH. And the peak output power is 150.33 μW , which is 358.3%

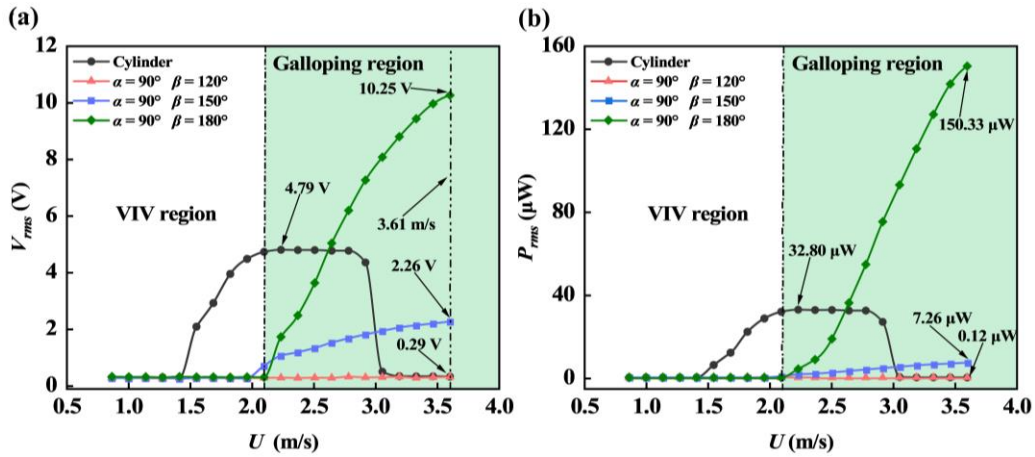
1 higher than that of the conventional VIVPEH.



2

3 **Figure 11.** Vibration characteristic of VIVPEH-S with $\alpha = 90^\circ$ and the conventional VIVPEH: (a)

4 Time history; (b) FFT analyses.



5

6 **Figure 12.** Harvesting performance of VIVPEH-S with $\alpha = 90^\circ$ and the conventional VIVPEH: (a)

7 Output voltage; (b) Output power.

8 To evaluate the harvesting performance of VIVPEH-S with $\alpha = 120^\circ$ and 150°
 9 and conduct the comparative analyses, the conventional VIVPEH is also adopted.

10 Figures 13 and 14 shows the output characteristics of the conventional VIVPEH and
 11 VIVPEH-S with $\alpha = 120^\circ \beta=150^\circ$, $\alpha = 120^\circ \beta = 180^\circ$, $\alpha = 150^\circ \beta = 180^\circ$ and the
 12 conventional VIVPEH at different wind speeds.

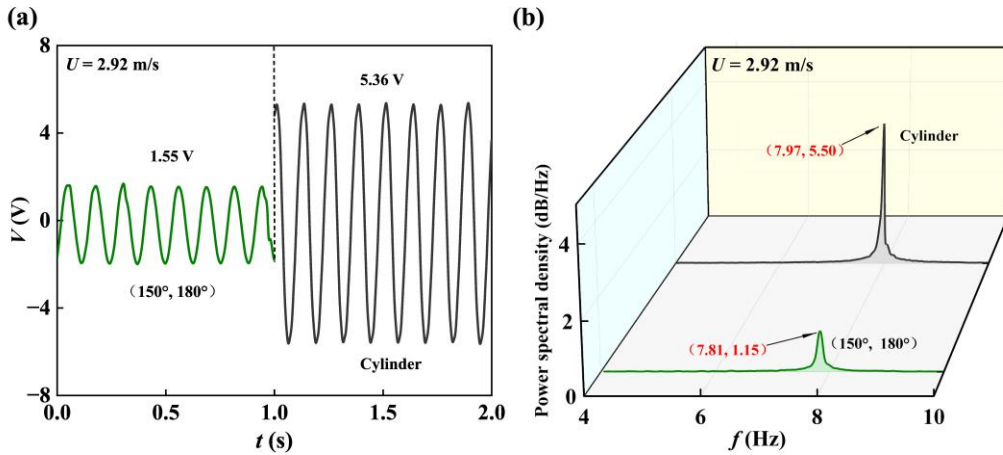


Figure 13. Vibration characteristic of VIVPEH-S with $\alpha = 150^\circ$ and the conventional VIVPEH: (a) Time history; (b) FFT analyses.

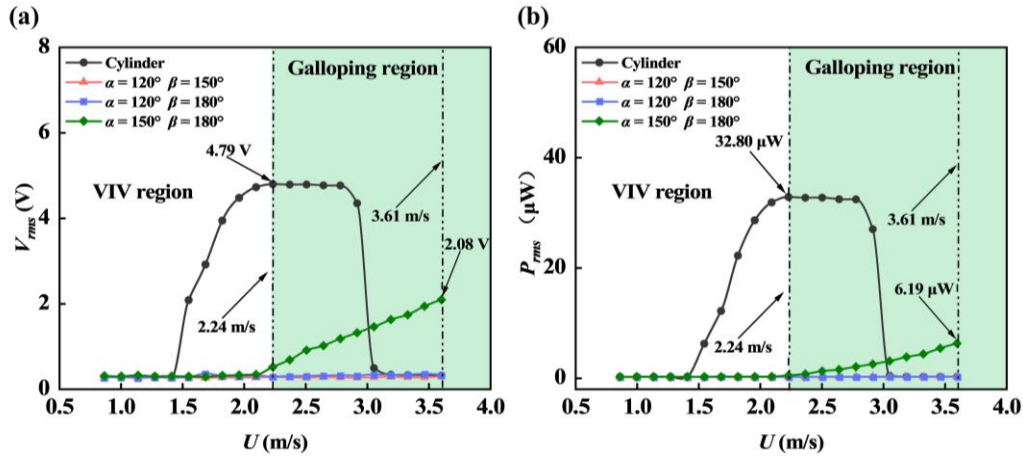
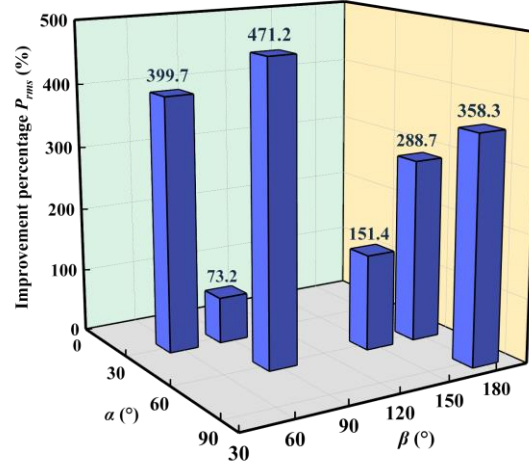


Figure 14. Harvesting performance of VIVPEH-S with $\alpha = 120^\circ$, 150° and the conventional VIVPEH: (a) Output voltage; (b) Output power.

1 The time history demonstrates that the vibration amplitude of VIVPEH-S with
 2 $\alpha=120^\circ$ and $\alpha=150^\circ$ is lower than the conventional VIVPEH. This means that the
 3 installation angles of $\alpha=120^\circ$ and $\alpha=150^\circ$ suppress the vibration response. Figure 13
 4 (b) FFT analyses show that the added asymmetrical splitter plates play a small
 5 influence on the vibration frequency. Figures 14 (a) and (b) show that the energy
 6 harvesting performance of VIVPEH-S with $\alpha=120^\circ$ is suppressed, and almost no
 7 voltage is generated. Although the output voltage and the output power of VIVPEH-S
 8 with $\alpha = 150^\circ$ and $\beta = 180^\circ$ are only 2.08 V and 6.19 μW , respectively. The output
 9 voltage only reaches about half of that of the conventional VIVPEH. It also means
 10 that the presence of asymmetrical splitter plates in the secondary case inhibits the
 11 energy harvesting performance.

12 To clearly demonstrate the enhancing performance by using two asymmetrical

1 splitter plates, Figure 15 illustrates the improvement percentage of output power at
 2 various installation angles. Therein, the improvement percentage of output power is
 3 calculated based on the conventional VIVPEH.



4
 5 **Figure 15.** Improvement percentage of the output power of different asymmetrical VIVPEH-S.

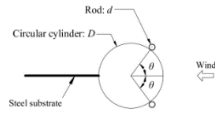
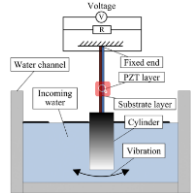
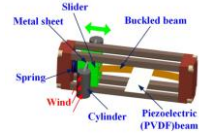
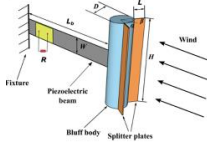
6 To sum up, Figure 15 shows that when $\alpha = 60^{\circ} \beta = 90^{\circ}$, $\alpha = 30^{\circ} \beta = 60^{\circ}$ and $\alpha =$
 7 $90^{\circ} \beta = 180^{\circ}$, the harvesting performance of VIVPEH-S can be largely enhanced, and
 8 improvement percentage of the output powers are increased by 471.2%, 399.7%, and
 9 358.3% compared with the conventional VIVPEH, respectively. In addition, when $\alpha =$
 10 $60^{\circ} \beta = 180^{\circ}$, $\alpha = 60^{\circ} \beta = 150^{\circ}$ and $\alpha = 30^{\circ} \beta = 90^{\circ}$, its energy output power is also
 11 significantly improved. Therefore, the certain installation angles of two asymmetrical
 12 splitter plates play a crucial role in improving energy harvesting efficiency.

13 To highlight better output characteristics of the proposed piezoelectric energy
 14 harvester attached to two asymmetrical splitter plates, Table 2 lists the performance
 15 comparisons of the referenced and proposed harvesters. The adopted piezoelectric
 16 energy harvesters are all subjected to the airflow for capturing wind energy. The
 17 performance criteria power density is defined as P_{ave}/V_m . Therein, P_{ave} refers to the
 18 average output power; V_m is the piezoelectric sheet volume.

19
 20
 21
 22
 23
 24

1
2

Table 2. Performance comparisons between the referred and proposed harvesters.

Reference	Airflow velocity (m/s)	Average power (mW)	Power density (mW/cm ³)	Configuration
Hu et al. [62]	6	0.072	0.202	
Song et al. [63]	0.35	0.084	0.302	
Zhang et al. [64]	14	0.062	0.471	
This work	3.6	0.187	0.623	

3 Table 2 demonstrates that the power density of the proposed harvester is up to
 4 ~~0.623~~ 623 mW/cm³, which shows the better output performance over others.
 5 Therefore, the proposed piezoelectric energy harvester attached to two asymmetrical
 6 splitter plates can promote the future actual applications in driving the
 7 microelectronics devices.”

8 **3. Simulation analyses of flow field characteristics and mode** 9 **conversion mechanism**

10 Based on the computational fluid dynamics software XFLOW platform (Dassault
 11 AG), this paper simulates the change of the vorticity of VIVPEH-S in the flow field,
 12 thereby further revealing the underlying mode conversion mechanism behind the
 13 above experimental phenomenon and improving the harvesting performance [65].
 14 Firstly, the convergence and accuracy of the flow field are ensured by numerical
 15 simulation of the two-dimensional cylinder. The computational domain of its CFD
 16 simulation is rectangular, with a length of 35 *D* and width of 20 *D*. The cylindrical

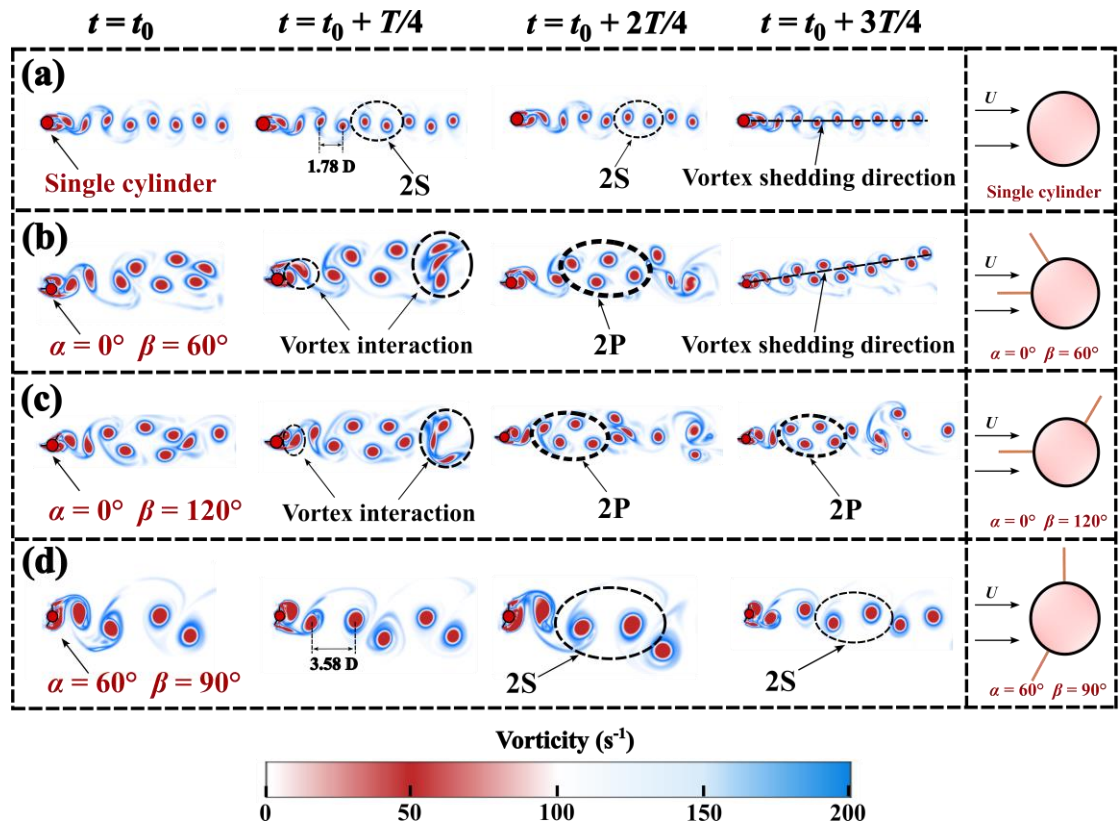
1 blunt body is located on the central axis of the flow field, and the distance from the
2 upstream boundary is $10 D$. The left and right boundaries of the flow field are velocity
3 inlet and flow outlet, respectively, and the upper and lower boundaries are set as a
4 wall. The fluid medium is set as air and the flow mode in the numerical calculation is
5 the single-phase forced incompressible model.

6 To weigh the computational accuracy and complexity in the convergence
7 investigation, three sizes of coarse, medium, and refined are selected, and their lattice
8 resolutions are 0.00185 m, 0.00175 m, and 0.00150 m, respectively. Three grid cell
9 numbers are 52834, 62870, and 80522, respectively. Table 3 lists the average values
10 of the drag coefficient C_D and the root mean square lift coefficient C_{Lrms} . The results
11 show that the computational results of C_D and C_{Lrms} converge gradually, and the
12 compromise between computational resources and accuracy can be achieved by using
13 a medium lattice size.

14 **Table 3.** The drag coefficient C_D and root mean square (RMS) lift coefficient C_{Lrms} .

Size	C_D	C_{Lrms}
Coarse	0.88742	0.142
Medium	1.02588	0.346
Refined	1.02810	0.357

15 To study the inherent influence of two asymmetrical splitter plates on the
16 vibration mechanism of the bluff body, the cylindrical control group and some
17 experimental models are selected for flow field vorticity analysis. Figure 16 illustrates
18 the vorticity contours obtained from CFD simulation to demonstrate the vortex
19 shedding processes. Therein, T represents the corresponding Strouhal vortex shedding
20 period.



1
2 **Figure 16.** Vorticity contours obtained from CFD simulation: (a) Single cylinder; (b)
3 Asymmetrical splitter plates with $\alpha = 0^\circ$ $\beta = 60^\circ$; (c) Asymmetrical splitter plates with $\alpha = 0^\circ$ $\beta = 120^\circ$;
4 (d) Asymmetrical splitter plates with $\alpha = 60^\circ$ $\beta = 90^\circ$.

5 Figure 16 (a) shows the vortex-shedding contours of the conventional VIVPEH.
6 The upper and lower boundary layers shed alternately with time, the wake shedding
7 pattern shows a stable “2S” mode [66-68], and the distance between the vortices is
8 about $1.78 D$. Figure 16 (b) illustrates the vortex shedding contours of VIVPEH-S
9 with $\alpha = 0^\circ$ and $\beta = 60^\circ$. The vortex is gradually generated along the splitter plates and
10 the cylindrical bluff body. Due to the existence of two asymmetrical splitter plates, the
11 motion process of the vortex on the lower half of the cylinder needs to flow a longer
12 distance than the upper half, which means that it takes longer to form the shedding
13 vortex behind the cylinder. Compared with the single cylindrical bluff body, the
14 alternating shedding of the upstream and downstream vortex cannot be well achieved,
15 which leads to the shortening of the distance between the downstream vortices and the
16 interaction such as collision and fusion. It finally causes the direction of the vortex
17 motion to deviate from the horizontal line. Due to the offset of the direction of the
18 vortex motion, the angle between the lift force and the vibration direction of the bluff
19 body is formed, thereby weakening the vibration intensity of the bluff body. This also

1 explains the main reason why the vibration of the experimental group is suppressed in
2 the entire experimental wind speed range. Figure 16 (c) illustrates the vortex shedding
3 contours of VIVPEH-S with $\alpha = 0^\circ$ and $\beta = 120^\circ$. The formation and shedding of the
4 vortex are still affected by the splitter plates, so that the distance between the wake
5 vortices becomes smaller, resulting in collision and fusion, the interaction between the
6 vortices is similar for $\alpha = 0^\circ$ and $\beta = 60^\circ$. However, for the formation mode of the
7 wake vortex, the vortex shedding shows a typical “2P” mode [69-71], which is not as
8 stable as the “2S” mode of a single cylinder and leads to a smaller amplitude vibration
9 of the bluff body during the experiment. The above analysis explains the internal
10 reason why the vibration is suppressed during the experiment from the perspective of
11 the motion form and the formed mode of the vortex. Then, the test group with the best
12 energy harvesting promotion effect in the experiment is selected for vortex shedding
13 mode analysis, as shown in Figure 16 (d). For VIVPEH-S with $\alpha = 60^\circ$ and $\beta = 90^\circ$,
14 due to the existence of the upper and lower asymmetrical splitter plates, the formation
15 of the vortex needs to move along the surface of the splitter plate and the bluff body
16 and fall off at the back. While different from the previous analysis, the frequency of
17 the vortex shedding ~~on~~ at the upper half surface and the lower plate surfaces is not
18 greatly affected, the entire vortex shedding mode is still in the typical “2S”. The
19 vortices will gather behind the splitter plate to form the larger vortex in the rear
20 compared to Figure 16 (a), and the distance between the vortices is also increased to
21 $3.58 D$. Compared with the cylindrical bluff body without the addition of the splitter
22 plates, two asymmetrical splitter plates with the certain angle can obtain a larger lift
23 force during the vibration of the bluff body, thereby promoting the energy harvesting
24 efficiency of VIVPEH-S. The intrinsic mechanism of the excellent energy harvesting
25 performance of the test group in the experimental testing. To sum up, the vortex
26 shedding analysis demonstrates that the internal mechanism for the effect of adding
27 asymmetrical splitter plates on energy harvesting in the experiment is explained by
28 the vortex shedding mode and motion process. The obtained simulation results
29 validate the above experimental results and reveal the vibration mode conversion
30 mechanism.

1 4. Conclusions

2 This paper proposed a novel piezoelectric energy harvester VIVPEH-S, for
3 converting the vibration mode and enhancing the energy harvesting efficiency. The
4 conceptual design of the energy harvester system was performed and the experimental
5 prototypes were constructed. The effects of the installation angle of two asymmetrical
6 splitter plates on the vibration characteristics and harvesting performance of
7 VIVPEH-S were experimentally investigated, and the vortex shedding characteristic
8 and mode conversion mechanism were revealed by CFD simulation. Some important
9 conclusions were drawn as follows:

10 (1) The installation angles of two asymmetrical splitter plates played a crucial
11 role in improving energy harvesting efficiency. The maximum output voltage of the
12 conventional VIVPEH is limited to 9.93 V at 0.865 m/s to 3.605 m/s. Compared with
13 the conventional VIVPEH, the energy harvesting efficiencies of VIVPEH-S with $\alpha =$
14 $30^\circ \beta = 60^\circ$, $\alpha = 30^\circ \beta = 90^\circ$, $\alpha = 60^\circ \beta = 90^\circ$, $\alpha = 60^\circ \beta = 150^\circ$, $\alpha = 60^\circ \beta = 180^\circ$, and
15 $\alpha = 90^\circ \beta = 180^\circ$ were promoted.

16 (2) A maximum enhancement ratio of the output power of VIVPEH-S with $\alpha =$
17 60° and $\beta = 90^\circ$ was up to 471.2% over the conventional VIVPEH. That is because
18 there existed the interaction of two asymmetrical splitter plates with the flow field,
19 and the vibration mode is finally transformed from VIV to galloping.

20 (3) Installing asymmetrical splitter plates can not only change the vortex
21 shedding mode, but also change the size and motion state of the vortex. When $\alpha = 0^\circ$
22 ($\beta = 60^\circ$ and $\beta = 120^\circ$), the vortex shedding mode was transformed from the
23 conventional “2S” to “2P” and moved to the vortex deviate from the horizontal
24 direction. When $\alpha = 60^\circ$ and $\beta = 90^\circ$, the vortex shedding mode behaved as the
25 conventional “2S” model, but the distance between the vortices was increased from
26 $1.78 D$ to $3.58 D$, and the size of the vortex was significantly increased.

27 (4) The flow field of VIVPEH-S revealed the mode conversion mechanism and
28 explained the promotion effect of the installation angle of two asymmetrical splitter
29 plates on the output characteristics.

30

1 CRediT authorship contribution statement

2 **Junlei Wang:** Writing- Original draft preparation, Methodology, Conceptualization,
3 Formal analysis. **Bing Xia:** Writing-Original draft preparation, Validation,
4 Methodology, Software. **Daniil Yurchenko:** Formal analysis, Writing- Reviewing and
5 Editing. **Grzegorz Litak:** Formal analysis, Writing- Reviewing and Editing. **Yong Li:**
6 Formal analysis, Writing- Reviewing and Editing. **Haigang Tian:** Formal analysis,
7 Writing- Reviewing and Editing.

8 Acknowledgments

9 This work was supported by the National Natural Science Foundation of China
10 (Grant No.: 51977196 and 52277227), China Postdoctoral Science Foundation
11 (2020T130557), Henan Province Science Foundation for Youths (202300410422),
12 and Program for Science & Technology Innovation Talents in Universities of Henan
13 Province (No. 23HASTIT010), the Ministry of Science and Higher Education in
14 Poland under the project DIALOG 0019/DLG/2019/10 in the years 2019-2022.

15 References

- 16 [1] A. Abdelkefi, N. Barsallo, L. Tang, Y. Yang, M. Hajj. Modeling, validation, and
17 performance of low-frequency piezoelectric energy harvesters. *Journal of Intelligent*
18 *Material Systems and Structures*. 2013; 25 (12):1429-1444.
- 19 [2] W. Sun, S. Jo, J. Seok. Development of the optimal bluff body for wind energy
20 harvesting using the synergetic effect of coupled vortex induced vibration and
21 galloping phenomena. *International Journal of Mechanical Sciences*. 2019; 156:435-
22 445.
- 23 [3] R. Naseer, H. Dai, A. Abdelkefi, L. Wang. Piezomagnetoelastic energy harvesting
24 from vortex-induced vibrations using monostable characteristics. *Applied Energy*.
25 2017; 203:142-153.
- 26 [4] H. Zou, W. Zhang, W. Li, K. Hu, K. Wei, Z. Peng, et al. A broadband compressive-
27 mode vibration energy harvester enhanced by magnetic force intervention approach.
28 *Applied Physics Letters*. 2017; 110 (16):163904.
- 29 [5] J. Wang, D. Fan, K. Lin. A review on flow-induced vibration of offshore circular
30 cylinders. *Journal of Hydrodynamics*. 2020; 32 (3):415-440.
- 31 [6] G. Luo, J. Xie, J. Liu, Q. Zhang, Y. Luo, M. Li, et al. Highly conductive,

-
- 1 stretchable, durable, breathable electrodes based on electrospun polyurethane mats
2 superficially decorated with carbon nanotubes for multifunctional wearable
3 electronics. *Chemical Engineering Journal*. 2023; 451:138549.
- 4 [7] J. Wang, D. Yurchenko, G. Hu, L. Zhao, L. Tang, Y. Yang. Perspectives in flow-
5 induced vibration energy harvesting. *Applied Physics Letters*. 2021; 119 (10):100502.
- 6 [8] N. Bosso, M. Magelli, N. Zampieri. Application of low-power energy harvesting
7 solutions in the railway field: a review. *Vehicle System Dynamics*. 2020; 59 (6):841-
8 871.
- 9 [9] K. Calautit, D. Nasir, B. Hughes. Low power energy harvesting systems: State of
10 the art and future challenges. *Renewable and Sustainable Energy Reviews*. 2021;
11 147:111230.
- 12 [10] D. Newell, M. Duffy. Review of Power Conversion and Energy Management for
13 Low-Power, Low-Voltage Energy Harvesting Powered Wireless Sensors. *IEEE*
14 *Transactions on Power Electronics*. 2019; 34 (10):9794-9805.
- 15 [11] L. Zhao, H. Zou, Z. Wu, Q. Gao, G. Yan, F. Liu, et al. Dynamically synergistic
16 regulation mechanism for rotation energy harvesting. *Mechanical Systems and Signal*
17 *Processing*. 2022; 169:108637.
- 18 [12] L. Weinstein, M. Cacan, P. So, P. Wright. Vortex shedding induced energy
19 harvesting from piezoelectric materials in heating, ventilation and air conditioning
20 flows. *Smart Materials and Structures*. 2012; 21 (4):045003.
- 21 [13] S. Kumar, C. Bose, S. Ali, S. Sarkar, S. Gupta. Investigations on a vortex induced
22 vibration based energy harvester. *Applied Physics Letters*. 2017; 111 (24):243903.
- 23 [14] J. Lee, B. Choi. Development of a piezoelectric energy harvesting system for
24 implementing wireless sensors on the tires. *Energy Conversion and Management*.
25 2014; 78:32-38.
- 26 [15] X. Xie, Q. Wang, N. Wu. Energy harvesting from transverse ocean waves by a
27 piezoelectric plate. *International Journal of Engineering Science*. 2014; 81:41-48.
- 28 [16] Z. Yang, J. Zu. Toward Harvesting Vibration Energy from Multiple Directions by
29 a Nonlinear Compressive-Mode Piezoelectric Transducer. *IEEE/ASME Transactions*
30 *on Mechatronics*. 2016; 21 (3):1787-1791.
- 31 [17] H.J. Zhu, J. Yao. Numerical evaluation of passive control of VIV by small
32 control rods. *Applied Ocean Research*. 2015; 51:93-116.
- 33 [18] J. Wang, G. Hu, Z. Su, G. Li, W. Zhao, L. Tang, et al. A cross-coupled dual-beam
34 for multi-directional energy harvesting from vortex induced vibrations. *Smart*
35 *Materials and Structures*. 2019; 28 (12):12LT02.
- 36 [19] X. Jiang, H. Zou, W. Zhang. Design and analysis of a multi-step piezoelectric
37 energy harvester using buckled beam driven by magnetic excitation. *Energy*
38 *Conversion and Management*. 2017; 145:129-137.
- 39 [20] A. Abdelkefi, M. Hajj, A. Nayfeh. Piezoelectric energy harvesting from
40 transverse galloping of bluff bodies. *Smart Materials and Structures*. 2013; 22
41 (1):015014.
- 42 [21] D. Akcabay, Y. Young. Hydroelastic response and energy harvesting potential of

-
- 1 flexible piezoelectric beams in viscous flow. *Physics of Fluids*. 2012; 24 (5):054106.
- 2 [22] M. Karimi, A. Karimi, R. Tikani, S. Ziaei-Rad. Experimental and theoretical
3 investigations on piezoelectric-based energy harvesting from bridge vibrations under
4 travelling vehicles. *International Journal of Mechanical Sciences*. 2016; 119:1-11.
- 5 [23] P. Carneiro, M. Soares dos Santos, A. Rodrigues, J. Ferreira, J. Simões, A.
6 Marques, et al. Electromagnetic energy harvesting using magnetic levitation
7 architectures: A review. *Applied Energy*. 2020; 260:114191.
- 8 [24] C. Williamson, R. Govardhan. Vortex-Induced Vibrations. *Annual Review of*
9 *Fluid Mechanics*. 2004; 36 (1):413-455.
- 10 [25] Z. Yang, L. Tang, L. Yu, K. Tao, K. Aw. Modelling and analysis of an out-of-
11 plane electret-based vibration energy harvester with AC and DC circuits. *Mechanical*
12 *Systems and Signal Processing*. 2020; 140:106660.
- 13 [26] M. Lallart, S. Pruvost, D. Guyomar. Electrostatic energy harvesting enhancement
14 using variable equivalent permittivity. *Physics Letters A*. 2011; 375 (45):3921-3924.
- 15 [27] L. Zhao, H. Zou, G. Yan, F. Liu, T. Tan, W. Zhang, et al. A water-proof
16 magnetically coupled piezoelectric-electromagnetic hybrid wind energy harvester.
17 *Applied Energy*. 2019; 239:735-746.
- 18 [28] G. Zhu, Z. Lin, Q. Jing, P. Bai, C. Pan, Y. Yang, et al. Toward large-scale energy
19 harvesting by a nanoparticle-enhanced triboelectric nanogenerator. *Nano Lett*. 2013;
20 13 (2):847-853.
- 21 [29] A. Barrero-Gil, D. Vicente-Ludlam, D. Gutierrez, F. Sastre. Enhance of Energy
22 Harvesting from Transverse Galloping by Actively Rotating the Galloping Body.
23 *Energies*. 2019; 13 (1):91.
- 24 [30] H. Zou, L. Zhao, Q. Wang, Q. Gao, G. Yan, K. Wei, et al. A self-regulation
25 strategy for triboelectric nanogenerator and self-powered wind-speed sensor. *Nano*
26 *Energy*. 2022; 95:106990.
- 27 [31] M. Hamlehdar, A. Kasaeian, M. Safaei. Energy harvesting from fluid flow using
28 piezoelectrics: A critical review. *Renewable Energy*. 2019; 143:1826-1838.
- 29 [32] Z. Yan, G. Shi, J. Zhou, L. Wang, L. Zuo, T. Tan. Wind piezoelectric energy
30 harvesting enhanced by elastic-interfered wake-induced vibration. *Energy Conversion*
31 *and Management*. 2021; 249:114820.
- 32 [33] H. Zou, W. Zhang, W. Li, K. Wei, Q. Gao, Z. Peng, et al. Design and
33 experimental investigation of a magnetically coupled vibration energy harvester using
34 two inverted piezoelectric cantilever beams for rotational motion. *Energy Conversion*
35 *and Management*. 2017; 148:1391-1398.
- 36 [34] G. Hu, K. Tse, M. Wei, R. Naseer, A. Abdelkefi, K. Kwok. Experimental
37 investigation on the efficiency of circular cylinder-based wind energy harvester with
38 different rod-shaped attachments. *Applied Energy*. 2018; 226:682-689.
- 39 [35] H. Jung, S. Lee. The experimental validation of a new energy harvesting system
40 based on the wake galloping phenomenon. *Smart Materials and Structures*. 2011; 20
41 (5):055022.
- 42 [36] A. Abdelkefi, J. Scanlon, E. McDowell, M. Hajj. Performance enhancement of

1 piezoelectric energy harvesters from wake galloping. *Applied Physics Letters*. 2013;
2 103 (3):033903.

3 [37] J. McCarthy, S. Watkins, A. Deivasigamani, S. John. Fluttering energy harvesters
4 in the wind: A review. *Journal of Sound and Vibration*. 2016; 361:355-377.

5 [38] H. Phan, D. Shin, H. Sang, T. Kang, P. Han, G. Kim, et al. Aerodynamic and
6 aeroelastic flutters driven triboelectric nanogenerators for harvesting broadband
7 airflow energy. *Nano Energy*. 2017; 33:476-484.

8 [39] Y. Yang, R. Zhou, Y. Ge, L. Zhang. Flutter Characteristics of Thin Plate Sections
9 for Aerodynamic Bridges. *Journal of Bridge Engineering*. 2018; 23 (1):04017121.

10 [40] E. de Langre. Frequency lock-in is caused by coupled-mode flutter. *Journal of*
11 *Fluids and Structures*. 2006; 22 (6-7):783-791.

12 [41] M. Bahmani, M. Akbari. Effects of mass and damping ratios on VIV of a circular
13 cylinder. *Ocean Engineering*. 2010; 37 (5-6):511-519.

14 [42] J. Wang, G. Zhao, M. Zhang, Z. Zhang. Efficient study of a coarse structure
15 number on the bluff body during the harvesting of wind energy. *Energy Sources, Part*
16 *A: Recovery, Utilization, and Environmental Effects*. 2018; 40 (15):1788-1797.

17 [43] W. Sun, D. Zhao, T. Tan, Z. Yan, P. Guo, X. Luo. Low velocity water flow energy
18 harvesting using vortex induced vibration and galloping. *Applied Energy*. 2019;
19 251:113392.

20 [44] K. Yang, T. Qiu, J. Wang, L. Tang. Magnet-induced monostable nonlinearity for
21 improving the VIV-galloping-coupled wind energy harvesting using combined cross-
22 sectioned bluff body. *Smart Materials and Structures*. 2020; 29 (7):07LT01.

23 [45] B. Zhang, B. Li, S. Fu, Z. Mao, W. Ding. Vortex-Induced Vibration (VIV)
24 hydrokinetic energy harvesting based on nonlinear damping. *Renewable Energy*.
25 2022; 195:1050-1063.

26 [46] G. Franzini, L. Bunzel. A numerical investigation on piezoelectric energy
27 harvesting from Vortex-Induced Vibrations with one and two degrees of freedom.
28 *Journal of Fluids and Structures*. 2018; 77:196-212.

29 [47] J. Vaseghi Amiri, G. Ghodrati Amiri, B. Ganjavi. Seismic vulnerability
30 assessment of multi-degree-of-freedom systems based on total input energy and
31 momentary input energy responses. *Canadian Journal of Civil Engineering*. 2008; 35
32 (1):41-56.

33 [48] B. Yan, N. Yu, H. Ma, C. Wu. A theory for bistable vibration isolators.
34 *Mechanical Systems and Signal Processing*. 2022; 167:108507.

35 [49] L. Zhang, H. Dai, A. Abdelkefi, L. Wang. Improving the performance of
36 aeroelastic energy harvesters by an interference cylinder. *Applied Physics Letters*.
37 2017; 111 (7):073904.

38 [50] O. Chabart, J. Lilien. Galloping of electrical lines in wind tunnel facilities.
39 *Journal of Wind Engineering and Industrial Aerodynamics*. 1998; 74-6:967-976.

40 [51] J. Xu-Xu, D. Vicente-Ludlam, A. Barrero-Gil. Theoretical study of the energy
41 harvesting of a cantilever with attached prism under aeroelastic galloping. *European*
42 *Journal of Mechanics B-Fluids*. 2016; 60:189-195.

-
- 1 [52] H. Zhu, J. Yao, Y. Ma, H. Zhao, Y. Tang. Simultaneous CFD evaluation of VIV
2 suppression using smaller control cylinders. *Journal of Fluids and Structures*. 2015;
3 57:66-80.
- 4 [53] J. Wang, L. Tang, L. Zhao, Z. Zhang. Efficiency investigation on energy
5 harvesting from airflows in HVAC system based on galloping of isosceles triangle
6 sectioned bluff bodies. *Energy*. 2019; 172:1066-1078.
- 7 [54] W. Xu, X. Zeng, Y. Wu. High aspect ratio (L/D) riser VIV prediction using wake
8 oscillator model. *Ocean Engineering*. 2008; 35 (17-18):1769-1774.
- 9 [55] T. Andrianne, R. Aryoputro, P. Laurent, G. Colson, X. Amandolèse, P. Hémon.
10 Energy harvesting from different aeroelastic instabilities of a square cylinder. *Journal*
11 *of Wind Engineering and Industrial Aerodynamics*. 2018; 172:164-169.
- 12 [56] L. Zhao, H. Zou, G. Yan, F. Liu, T. Tan, K. Wei, et al. Magnetic coupling and
13 flextensional amplification mechanisms for high-robustness ambient wind energy
14 harvesting. *Energy Conversion and Management*. 2019; 201:112166.
- 15 [57] J. Song, G. Hu, K. Tse, S. Li, K. Kwok. Performance of a circular cylinder
16 piezoelectric wind energy harvester fitted with a splitter plate. *Applied Physics*
17 *Letters*. 2017; 111 (22):223903.
- 18 [58] J. Wang, S. Zhou, Z. Zhang, D. Yurchenko. High-performance piezoelectric wind
19 energy harvester with Y-shaped attachments. *Energy Conversion and Management*.
20 2019; 181:645-652.
- 21 [59] J. Wang, S. Gu, A. Abdelkefi, C. Bose. Enhancing piezoelectric energy
22 harvesting from the flow-induced vibration of a circular cylinder using dual splitters.
23 *Smart Materials and Structures*. 2021; 30 (5):05LT01.
- 24 [60] C. Mannini, A. Marra, G. Bartoli. VIV-galloping instability of rectangular
25 cylinders: Review and new experiments. *Journal of Wind Engineering and Industrial*
26 *Aerodynamics*. 2014; 132:109-124.
- 27 [61] C. Mannini, A. Marra, G. Bartoli. Experimental investigation on VIV-galloping
28 interaction of a rectangular 3:2 cylinder. *Meccanica*. 2014; 50 (3):841-853.
- 29 [62] G. Hu, K.T. Tse, K.C.S. Kwok, J. Song, Y. Lyu. Aerodynamic modification to a
30 circular cylinder to enhance the piezoelectric wind energy harvesting. *Applied Physics*
31 *Letters*. 2016; 109 (19).
- 32 [63] R. Song, X. Shan, F. Lv, T. Xie. A study of vortex-induced energy harvesting
33 from water using PZT piezoelectric cantilever with cylindrical extension. *Ceramics*
34 *International*. 2015; 41:S768-S773.
- 35 [64] J. Zhang, J. Zhang, C. Shu, Z. Fang. Enhanced piezoelectric wind energy
36 harvesting based on a buckled beam. *Applied Physics Letters*. 2017; 110 (18).
- 37 [65] J. Wang, C. Zhang, G. Hu, X. Liu, H. Liu, Z. Zhang, et al. Wake galloping energy
38 harvesting in heat exchange systems under the influence of ash deposition. *Energy*.
39 2022; 253:124175.
- 40 [66] A. Munir, M. Zhao, H. Wu, F. Tong. Flow-induced vibration of a rotating circular
41 cylinder at high reduced velocities and high rotation rates. *Ocean Engineering*. 2021;
42 238:109562.

-
- 1 [67] K. Sourav, D. Kumar, S. Sen. Undamped transverse-only VIV of a diamond
2 cylinder at low Reynolds numbers. *Ocean Engineering*. 2020; 197:106867.
- 3 [68] L. Ding, L. Zhang, M. Bernitsas, C. Chang. Numerical simulation and
4 experimental validation for energy harvesting of single-cylinder VIVACE converter
5 with passive turbulence control. *Renewable Energy*. 2016; 85:1246-1259.
- 6 [69] F. Xie, J. Deng, Q. Xiao, Y. Zheng. A numerical simulation of VIV on a flexible
7 circular cylinder. *Fluid Dynamics Research*. 2012; 44 (4):045508.
- 8 [70] D. Yu, C. Jianping, C. Yizhong, Y. Ma. Prediction of the VIV Responses Based
9 on the Numerical Solutions of Controlled Motion. *Shock and Vibration*. 2021;
10 2021:1-14.
- 11 [71] D. Lucor, J. Foo, G. Karniadakis. Vortex mode selection of a rigid cylinder
12 subject to VIV at low mass-damping. *Journal of Fluids and Structures*. 2005; 20
13 (4):483-503.
- 14